Journal of Alloys and Compounds 695 (2017) 1523–1527

Contents lists available at ScienceDirect

Journal of Alloys and Compounds

journal homepage: http://www.elsevier.com/locate/jalcom

Correlation between native defects and morphological, structural and optical properties of ZnO nanostructures

Limei Lin [a, b, *], Jinyang Liu [a, b], Jing Lv [c], Shuangjuan Shen [a, b], Xiaoping Wu [a, b], Daochu Wu [a], Yan Qu [a, b], Weifeng Zheng [a, b], Fachun Lai [a, b]

[a] Fujian Provincial Key Laboratory of Quantum Manipulation and New Energy Materials, College of Physics and Energy, Fujian Normal University, Fuzhou, 350117, PR China
[b] Fujian Provincial Collaborative Innovation Center for Optoelectronic Semiconductors and Efficient Devices, Xiamen, 361005, PR China
[c] School of Physics and Mechanical & Electrical Engineering, Longyan University, Longyan, 364000, PR China

ARTICLE INFO

Article history:
Received 7 April 2016
Received in revised form
23 September 2016
Accepted 29 October 2016
Available online 1 November 2016

Keywords:
ZnO nanostructure
Raman spectra
Photoluminescence
Native defect

ABSTRACT

ZnO nanostructures are synthesized using chemical vapor deposition method. Well-distributed ZnO nanowires, nanogrenades and nanoislands are obtained by altering the temperature of joining the reactant gas O_2 from 550 to 570 and 600 °C, respectively. The structural properties are derived from the X-ray diffraction patterns and Raman spectra. It is indicated that all the samples are c-oriented wurtzite ZnO. Photoluminescence spectra also indicate that ZnO nanogrenades present fewer native defects because of their lower relative intensities of visible to ultraviolet emissions (1.1) than that of ZnO nanowires (3.1) and nanoislands (1.9). The visible emission of photoluminescence spectrum is divided into green and yellow luminescence which are attributed to defects of oxygen vacancy and surface disorder, respectively. And it is found different proportions of oxygen vacancy and surface disorder of variform ZnO nanostructures.

1. Introduction

Recently, nanosize ZnO materials have attracted a great deal of attentions due to their potential applications in optoelectronic devices, such as solar cells [1], gas sensors [2], light emitters [3] and photodetectors [4], and so on. These attractive applications have led to extensive studies of basic properties of ZnO nanostructures, especially understanding the roles of native defects which dominate the performance of ZnO [5].

Controlling of intrinsic defects and corresponding effects on vibrational properties are of paramount importance in applications of ZnO. However, controlling the defect density and maintaining a balance among various defect types is quite challenging. The intrinsic defects of ZnO are commonly defined as oxygen and zinc vacancies (V_O and V_{Zn}), interstitials (O_i and Zn_i), and antisites (O_{Zn} and Zn_O) [5]. Generally, samples with different native defects can be obtained by properly controlling the growth or post-treatment conditions which can be classified into the O-rich and Zn-rich environments [6–11]. For example, Liu et al. have found that densities of oxygen vacancies and zinc vacancies change by annealing at different temperatures in open air, which mainly attributes to thermal effect, annealing environment and mechanical damages [8]. ZnO nanostructures with different defect properties have been synthesized by a common chemical vapor deposition (CVD) method through changing substrate temperature [11,12], relative flow rate of carrier gas to reactant gas [13,14], different growth time [15], and so on.

ZnO defects can be characterized by different technological methods, and photoluminescence (PL) is one of the most relevant methods. Typically, PL spectra of ZnO often present two emission bands in the ultraviolet (UV) and visible (VIS) regions. The UV emission also named near band emission attributed to the band–edge transition or the free exciton recombination is usually considered as a characteristic emission of ZnO [9]. And the VIS emission is universally associated with the native defects in ZnO. Although extensive controversies on clearing defect centers have existed for more than two decades, and unambiguous electron

* Corresponding author. Fujian Provincial Key Laboratory of Quantum Manipulation and New Energy Materials, College of Physics and Energy, Fujian Normal University, Fuzhou, 350117, PR China.
E-mail address: linlm@fjnu.edu.cn (L. Lin).

http://dx.doi.org/10.1016/j.jallcom.2016.10.292
0925-8388/

transitions are not yet known in detail. Take the green emission in the visible region for example, it has been attributed to transitions with defects of V_O [10,11,16–18], V_{Zn} [6,18,19], Zn_i [20], or O_{Zn} [21], and so on.

In this work, we have employed CVD method to synthesize ZnO nanostructures by simply changing the temperature (T_{O2}) while the oxygen gas joins into the carrier gas, which has not been reported before. With different T_{O2}, it is obtained ZnO with variously morphological, structural and optical properties.

2. Experimental details

ZnO nanostructures were prepared on ZnO:Al (AZO) substrate by CVD method. AZO thin film with thickness of ~350 nm was deposited on quartz by radio frequency magnetron sputtering [22]. Zn powder (0.10 g, 4 N) and AZO substrate were placed in center of a single zone tube furnace with separation of 6.5 cm. The furnace tube was evacuated to less than 10 Pa using a mechanical pump. Then the furnace tube was heated to 500 °C with uniform heating rate of 20 °C/min, and carrier gas Ar of 100 sccm flowed into the furnace tube. Next, the tube continued to heat up. And when the temperature reached up to 550, 570 or 600 °C, the reactant gas O_2 of 2.0 sccm joined to Ar. After the temperature increased to 600 °C and held for 3 min, Ar and O_2 were closed and the furnace tube was cooled naturally. With different temperature of joining O_2, samples of various properties were prepared.

The morphological properties were investigated by a field emission scanning electron microscope (SEM-SU8010, Hitachi). The crystallinity properties were characterized by an X-ray diffraction (Mini Flex-II, Rigaku) using Cu K_α radiation ($\lambda_{K\alpha}$ = 0.1542 nm). Photoluminescence properties and Raman spectra were obtained on a spectrophotometer (LabRAM HR Evolution, Horiba scientific) equipped with excitation sources of 325 nm and 532 nm, respectively.

3. Results and discussion

3.1. Surface morphology

A series of samples are synthesized using CVD method with identical growth conditions except T_{O2}. Fig. 1(a), (b) and (c) give the top-view SEM images of samples prepared with T_{O2} of 550, 570 and 600 °C, respectively. These top-view images clearly show that well-distributed and variform ZnO nanostructures are obtained by simply changing T_{O2}. To resolve the detail information among the growth process, cross-section SEM images of ZnO nanostructures have been investigated and shown in Fig. 1(d).

Fig. 1(d) shows that there is a thin ZnO buffer layer with thickness of ~50 nm between the nanostructures and AZO substrate. Because Zn particles carried by Ar re-evaporate from the AZO surface at such high substrate temperature, and it can hardly form an effective buffer layer on AZO until O_2 joins. When O_2 turns into the system at 550 °C (T_{O2} of 550 °C), ZnO forms on AZO and re-evaporates difficultly because of its high melting point. Meanwhile, Zn source reacts with O_2 and forms a protective ZnO thin layer which constrains the evaporation of Zn source. And then with temperature going up, slender and dense ZnO nanowires (ZnO NW) are prepared with diameter of 34 ± 4 nm and height of 310 ± 20 nm. When T_{O2} increases to 570 °C, the more quantity of Zn vapor the bigger ZnO nucleating on AZO. So sparse and bigger ZnO nanorods can be observed. However, the evaporation rate of Zn source goes up with increasing of temperature, then the nanorods enlarge until protective ZnO thin layer of Zn source building. Finally, hexagonal ZnO nanogrenades (ZnO NG) with shape of a handle grenade is observed (Fig. 1(d)). As T_{O2} goes up to 600 °C, high temperature and sufficient Zn vapor result in a large quantity of ZnO. Then it is found large and irregular ZnO nanoislands (ZnO NI) on AZO. In conclusion, with simply changing the temperature of joining O_2 to the CVD system, well-distributed ZnO nanowires, hexagonal nanogrenades and big nanoislands can be obtained.

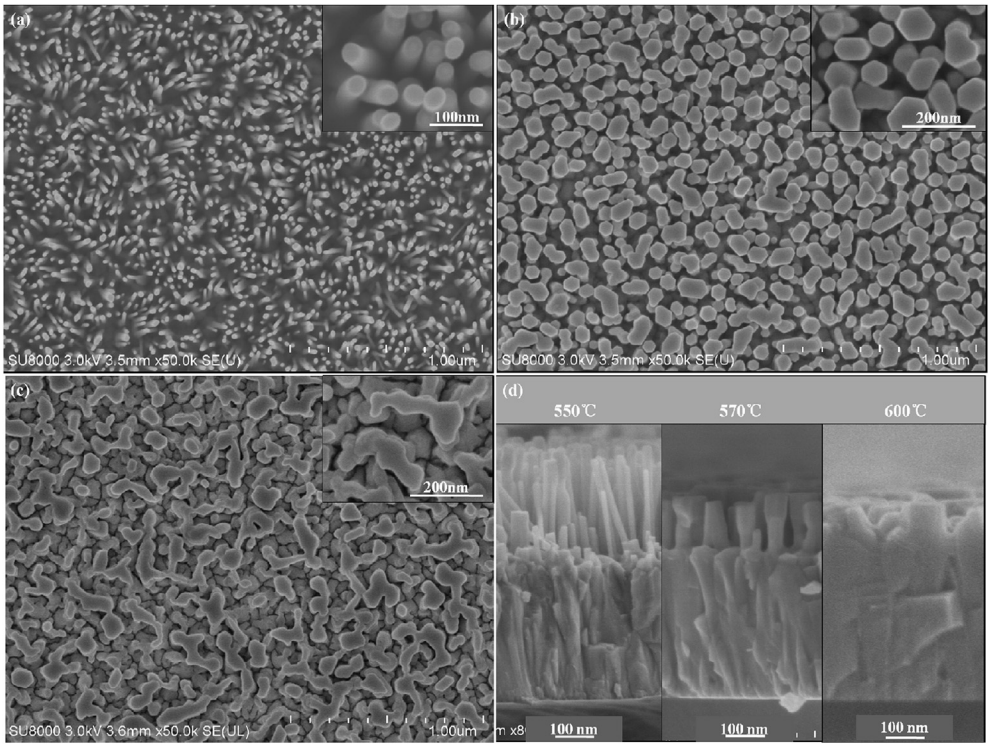

Fig. 1. Low and high (inset) magnification top-view SEM images of ZnO nanostructures prepared with T_{O2} of 550 °C (a), 570 °C (b) and 600 °C (c), and cross-section SEM images (d).

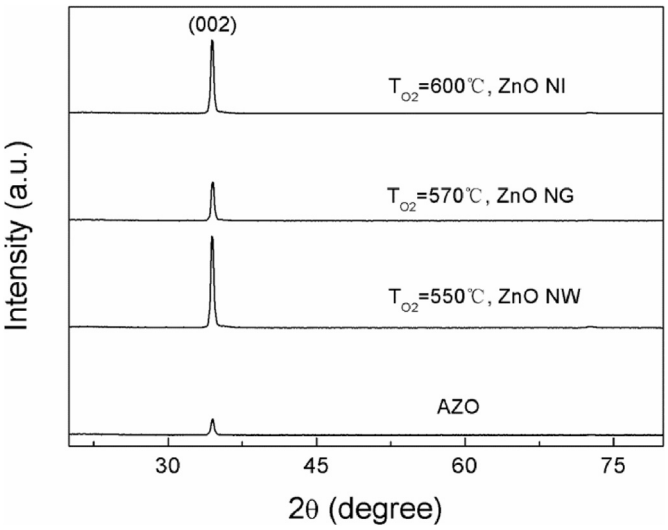

Fig. 2. XRD patterns of AZO substrate and ZnO nanostructures.

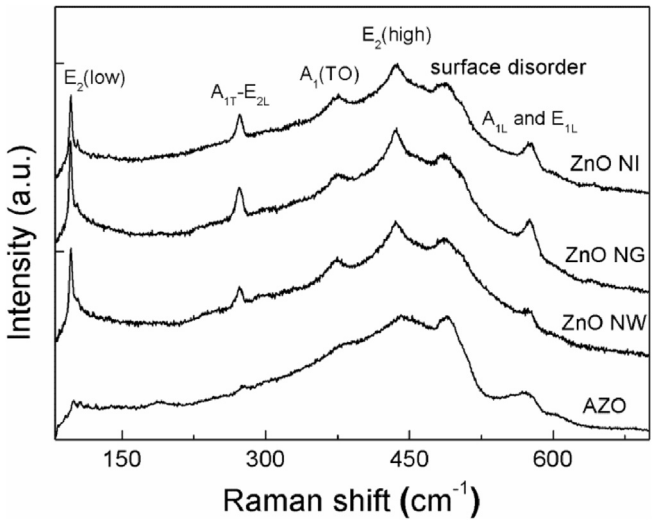

Fig. 3. Raman spectra of AZO substrate and ZnO nanostructures.

3.2. Structural properties

Fig. 2 illustrates the XRD patterns of AZO substrate and ZnO nanostructures grown with different T_{O2}. Only XRD peak corresponding to wurtzite ZnO (002) plane can be seen, revealing high crystallinity and c-axis preferential orientation of all the samples [23]. The mean crystallite size can be estimated via the Scherrer equation using the full width at half-maximum (FWHM) of the (002) peak. And the mean crystallite size of AZO, ZnO NW, NG and NI is 25.6, 28.2, 29.1 and 28.6 nm respectively. The weaker intensity of (002) peak and smaller crystallite size in spite of a great quantity AZO, which means poorer crystallinity of AZO than ZnO nanostructures. It is also found that the crystallinity of ZnO NG is a little better than other nanostructures.

To obtain more structural details of the samples, room-temperature Raman spectra are investigated and presented in Fig. 3. Meanwhile Raman peaks have been identified reference to Raman modes of ZnO bulk and listed in Table 1. In Fig. 3, ZnO nanostructures shows higher peak intensities than AZO, which means better crystallinity and more perfect lattice structure of ZnO nanostructures than AZO. And all the samples present a characteristic of wurtzite structure, because of the presence of the E_2(low) mode around 97 cm^{-1} associated with the vibration of Zn sublattice and E_2(high) mode at 437 cm^{-1} of oxygen atom [13,15,21,24,25]. In addition, Compared to ZnO NW and NI, ZnO NG shows stronger intensity of both E_2 modes because of its better crystal quality. These results confirm with the XRD analyses.

The presence of other modes refers to crystal disorder or defects. According to Raman selection rule, the A_1(LO) mode around 574 cm^{-1} is associated with crystalline property of wurtzite structure ZnO and only allowed with ZnO orientation in the c-axis [13,25]. The E_1(LO) mode at 583 cm^{-1} is close to the A_1(LO) mode and allowed while c-axis orientation of ZnO is perpendicular to normal incident laser. And there are some tilted nanostructures cannot well define with the incident laser direction. So, we assume that Raman peak around 577 cm^{-1} of all the samples must be a combination of A_1(LO) and E_1(LO) modes [13,15,21,24,25]. Peak around 270 cm^{-1} may be attributed to multiple phones of A_1(TO) and E_2(low). In addition, A_1(TO) mode around 380 cm^{-1} refers to the phone localization induced by native defects of ZnO [15]. It is obviously fewer native defects of ZnO NG, which results from the lower A_1(TO) intensities of ZnO NW than ZnO NG and NI. A broad peak around 495 cm^{-1} appears in all the samples, which has associated to surface phonon mode from surface disorder [25]. And as T_{O2} increases the 495 cm^{-1} peak shows a redshift, which may be attributed to change of nanostructure morphology. In Table 1, it also illustrates that E_2 and A_1(TO) modes present redshifts compared to theory value of ZnO bulk, which ordinarily connect to residual stress or crystal disorder in the ZnO nanostructures [15,21,24].

In short summary, all the ZnO nanostructures reveal a characteristic of c-oriented wurtzite structure, and ZnO NG prepared at T_{O2} of 570 °C possess better crystal quality and fewer native defects.

3.3. Photoluminescence properties

Room-temperature PL spectra in function of energy of all the samples are given in Fig. 4. In Fig. 4(d), poor crystallinity AZO shows two weak emissions, one is a UV emission with center at 3.33 eV and intensity of 3.6 a.u., the other one is a green luminescence with center at 2.25 eV and intensity of 9.7 a.u.. And the intensities of the PL spectra shown in Fig. 4(a)–(c) reach up to 350 a.u., so it is considered that the present emissions in Fig. 4(a)–(c) mainly correspond to ZnO nanostructures.

The PL spectra of ZnO nanostructures typically exhibit a narrow UV emission and a broad VIS emission. The UV emission centered at 3.28 eV connects to recombination of free exciton, and the VIS

Table 1
Raman mode positions of ZnO nanostructures respect toT_{O2}.

T_{O2} (°C)	Sample	Raman peak positions (cm^{-1})					
550	ZnO NW	97 (−4)	273	373 (−7)	436 (−1)	495	576
570	ZnO NG	96 (−5)	272	375 (−5)	435 (−2)	493	576
600	ZnO NI	97 (−4)	273	374 (−6)	436 (−1)	492	577
Theory		101		380	437		574/583
Peak identity		E_2(low)	A_{1T} - E_{2L}	A_1(TO)	E_2(high)	Surface disorder	A_{1L} and E_{1L}

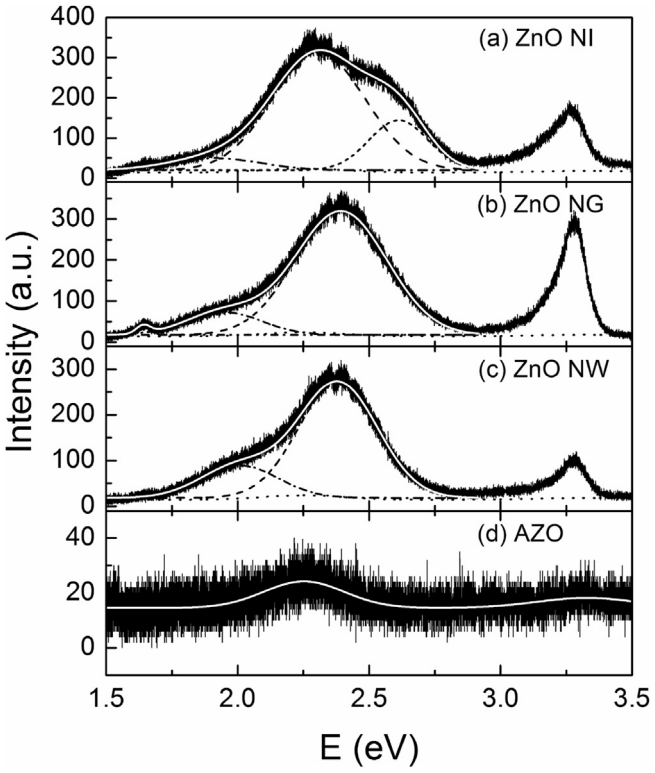

Fig. 4. Room-temperature photoluminescence spectra of AZO substrate and ZnO nanostructures.

increasing T_{O2}, the relative intensities of YL to UV decrease, which may result from enlarging of the nanostructures. Red shift of the yellow peak appears with increasing T_{O2}, matching with the red shift of Raman peak around 495 cm^{-1} associated with surface disorder. A weak blue-green emission (short dash line) at 2.61 eV ascribed to transition from the extended states of Zn_i to valence band has been derived from PL spectrum of ZnO NI, which might result from the maximum Zn_i generated in the highest concentration of Zn vapor [9,20].

Meanwhile, it can be deduced from the relative intensities listed in Table 2 that ZnO NW has more V_O and surface disorder defects, but fewer of ZnO NG. Calculation the relative intensities of GL to YL, results of ZnO NW, NG and NI are 3.6, 5.4 and 9.7, respectively. It is found that with increasing of T_{O2} the proportion of V_O in native defects of respective nanostructures rises, but the proportion of surface disorder defect reduces because size of the nanostructures enlarges.

4. Conclusions

ZnO nanostructures were synthesized using CVD method by simply changing the temperature T_{O2} while the reactant gas O_2 joins to carrier gas Ar. When O_2 joins, ZnO nanostructures form and grow on AZO substrate, meanwhile a protective ZnO film forms on Zn source. With different T_{O2}, ZnO nanowires, nanogrenades, and nanoislands are obtained. All the samples are c-oriented wurtzite ZnO nanostructures, and ZnO nanogrenades present better crystallinity. It is demonstrated that ZnO nanowires shows more V_O and surface disorder defects because of their high surface-volume ratio, and ZnO nanogrenades possess less crystal disorder and native defects. With increasing of T_{O2}, the proportion of V_O in native defects of respective nanostructures rises, but the proportion of surface disorder defect reduces. The nanostructures of various properties possess universality for designing various nanodevices and match widespread applications.

Table 2
PL peaks and relative intensity of ZnO nanostructures respect to T_{O2}.

T_{O2} (°C)	Sample	PL peaks (nm) and relative intensity					
550	ZnO NW	3.1	3.28, 1		2.38, 2.6	2.01, 0.74	
570	ZnO NG	1.1	3.28, 1		2.39, 1.1	1.95, 0.19	1.64, 0.068
600	ZnO NI	1.9	3.26, 1	2.61, 0.74	2.31, 1.7	1.91, 0.18	
Peak identity		I_{VIS}/I_{UV}	FX	ex-Zn_i	V_O	Surface disorder	Second order of UV

emission refers to native defects of ZnO [16]. The relative intensities I_{VIS}/I_{UV} of all the nanostructures are calculated and listed in Table 2, and I_{VIS}/I_{UV} of ZnO NW, NG and NI is 3.1, 1.1, and 1.9, respecttively. The lower I_{VIS}/I_{UV} responses to better crystal quality and fewer defects. Therefore, it can be deduced that ZnO NG possesses higher crystallinity and ZnO NW has more native defects, which also matches with the morphological and structural results.

To provide direct insight into the PL emission mechanisms, visible emission of these spectral features with emission from AZO (dot lines in Fig. 4(a)–(c)) taken off have been divided by fitting multiple Guass peaks and plotted in Fig. 4 [26]. The obtained results of the Guass peak positions and relative intensities to UV are also shown in Table 2. As exhibited in Fig. 4(c), the PL spectrum of ZnO NW in the visible region is resolved into two emission bands of green luminescence (GL, dash line) centered at 2.38 eV and broad yellow luminescence (YL, dash dot line) at 2.01 eV. The GL is often attributed to the transition from conduction band to the deep levels of V_O include singly and double charged oxygen vacancy [21]. V_O has the lowest formation energy in the Zn-rich condition, and then visible emission of all the samples be dominated by GL [5]. The yellow peak with low intensity and broad pattern is unlikely to be related to intrinsic defects, and it is prominent in ZnO NW which shows more surface-volume ratio [5,21]. So, the yellow peak must attribute to surface disorder in ZnO nanostructures [11]. With

Acknowledgments

This work was supported by the National Science Foundation of China (No. 11374052) and Fujian Province (No. 2013J01174), and the Science Foundation of Educational Department of Fujian Province of China (No. JB13023 and No. JA13075).

References

[1] C.P. Liu, Z.H. Chen, H.E. Wang, S.K. Jha, W.J. Zhang, I. Bello, J.A. Zapien, Enhanced performance by incorporation of zinc oxide nanowire array for organic-inorganic hybrid solar cells, Appl. Phys. Lett. 100 (24) (2012) 243102.
[2] H. Bian, S. Ma, A. Sun, X. Xu, G. Yang, S. Yan, J. Gao, Z. Zhang, H. Zhu, Improvement of acetone gas sensing performance of ZnO nanoparticles, J. Alloy. Compd. 658 (2016) 629–635.
[3] H. Long, S.Z. Li, X.M. Mo, H.N. Wang, H.H. Huang, Z. Chen, Y.P. Liu, G.J. Fang, Electroluminescence from ZnO-nanorod-based double heterostructured light-emitting diodes, Appl. Phys. Lett. 103 (12) (2013) 123504.
[4] S. Parka, S. Kima, G.J. Suna, D.B. Byeona, S.K. Hyuna, W.I. Leeb, C. Leea, ZnO-core ZnSe-shell nanowire UV photodetector, J. Alloy. Compd. 658 (2016)

459–464.
[5] A. Janotti, C.G. Van de Walle, Native point defects in ZnO, Phys. Rev. B 76 (16) (2007) 165202.
[6] L. Ke, S.C. Lai, J.D. Ye, V.L. Kaixin, S.J. Chua, Point defects analysis of zinc oxide thin films annealed at different temperatures with photoluminescence, Hall mobility, and low frequency noise, J. Appl. Phys. 108 (8) (2010) 084502.
[7] P. Tiwari, H. Srivastava, A.K. Srivastava, S.K. Deb, A comparative study on the growth of ZnO nanorods by annealing method in different environments, J. Alloy. Compd. 611 (2014) 117–124.
[8] J. Liu, Y. Zhao, Y.J. Jiang, C.M. Lee, Y.L. Liu, G.G. Siu, Identification of zinc and oxygen vacancy states in nonpolar ZnO single crystal using polarized photoluminescence, Appl. Phys. Lett. 97 (23) (2010) 231907.
[9] H. Zeng, G. Duan, Y. Li, S. Yang, X. Xu, W. Cai, Blue luminescence of ZnO nanoparticles based on non-equilibrium processes: defect origins and emission controls, Adv. Funct. Mater. 20 (4) (2010) 561–572.
[10] L.M. Kukreja, P. Misra, J. Fallert, D.M. Phase, H. Kalt, Correlation of spectral features of photoluminescence with residual native defects of ZnO thin films annealed at different temperatures, J. Appl. Phys. 112 (1) (2012) 013525.
[11] T. Nguyen, N.T. Tuan, V.D. Nguyen, N.D. Cuong, N.D.T. Kien, P.T. Huy, V.H. Nguyen, D.H. Nguyen, Near-infrared emission from ZnO nanorods grown by thermal evaporation, J. Luminescence 156 (2014) 199–204.
[12] J. Li, Q. Zhang, H. Peng, H.O. Everitt, L. Qin, J. Liu, Diameter-controlled Vapor–Solid epitaxial growth and properties of aligned ZnO nanowire arrays, J. Phys. Chem. C 113 (10) (2009) 3950–3954.
[13] T. Ngo-Duc, K. Singh, M. Meyyappan, M.M. Oye, Vertical ZnO nanowire growth on metal substrates, Nanotechnology 23 (19) (2012) 194015.
[14] S. Li, X. Zhang, B. Yan, T. Yu, Growth mechanism and diameter control of well-aligned small-diameter ZnO nanowire arrays synthesized by a catalyst-free thermal evaporation method, Nanotechnology 20 (49) (2009) 495604.
[15] Y. Zhang, Z. Wang, F. Lu, Y. Zhang, Y. Xiao, L. Zhang, Property modulation of zinc oxide hierarchical architectures in photoluminescence and Raman scattering, Appl. Phys. Lett. 89 (11) (2006) 113110.
[16] X.L. Wu, G.G. Siu, C.L. Fu, H.C. Ong, Photoluminescence and cathodoluminescence studies of stoichiometric and oxygen-deficient ZnO films, Appl. Phys. Lett. 78 (16) (2001) 2285–2287.
[17] K. Vanheusden, C.H. Seager, W.L. Warren, D.R. Tallant, J.A. Voigt, Correlation between photoluminescence and oxygen vacancies in ZnO phosphors, Appl. Phys. Lett. 68 (3) (1996) 403–405.
[18] M. Wang, Y. Zhou, Y. Zhang, E. Jung Kim, S. Hong Hahn, S. Gie Seong, Near-infrared photoluminescence from ZnO, Appl. Phys. Lett. 100 (10) (2012) 101906.
[19] Y.W. Heo, D.P. Norton, S.J. Pearton, Origin of green luminescence in ZnO thin film grown by molecular-beam epitaxy, J. Appl. Phys. 98 (7) (2005) 073502.
[20] F. Kayaci, S. Vempati, I. Donmez, N. Biyikli, T. Uyar, Role of zinc interstitials and oxygen vacancies of ZnO in photocatalysis: a bottom-up approach to control defect density, Nanoscale 6 (17) (2014) 10224–10234.
[21] P.K. Giri, S. Bhattacharyya, D.K. Singh, R. Kesavamoorthy, B.K. Panigrahi, K.G.M. Nair, Correlation between microstructure and optical properties of ZnO nanoparticles synthesized by ball milling, J. Appl. Phys. 102 (9) (2007) 093515.
[22] L. Fan, F. Lai, L. Lin, Y. Pei, Y. Qu, Investigation of conductive and transparent Al-doped ZnO/metal dual-layer films by magnetron sputtering, SPIE Conf. 7282 (2009) 728216.
[23] T.M.K. Thandavan, C.S. Wong, S.M.A. Gani, R.M. Nor, Photoluminescence properties of un-doped and Mn-doped ZnO nanostructures, Mater. Express 4 (6) (2014) 475–482.
[24] P. Ghosh, A.K. Sharma, Effect of substrate temperature on the growth of pulsed-laser deposited ZnO nanostructures, Appl. Phys. A 116 (8) (2014) 1877–1884.
[25] A.J. Cheng, Y. Tzeng, H. Xu, S. Alur, Y. Wang, M. Park, T.H. Wu, C. Shannon, D.J. Kim, D. Wang, Raman analysis of longitudinal optical phonon-plasmon coupled modes of aligned ZnO nanorods, J. Appl. Phys. 105 (7) (2009) 073104.
[26] G. Blasse, B.C. Grabmaier, Luminescent Materials, Springer, Berlin, 1994.